RESEARCH PAPER

Annealing Effects on Structure, Surface Morphology and Optical Properties of Cu-Doped CdO_x Thin Films Grown by Spray Pyrolysis

Nooralhuda Hassan, Zainab Naji Jaf, Hanaa Ibrahem Mohammed, Mohammed Hamid Mustafa, Hussein Ali Jan Miran*

* *Hussein.a.j@ihcoedu.uobaghdad.edu.iq*

Department of Physics, College of Education for Pure Science-Ibn Al-Haitham, University of Baghdad, Baghdad, Iraq

Received: April 2025 **Revised: May 2025** **Accepted: June 2025**
DOI: 10.22068/ijmse.3991

Abstract: *This work reports the influence of Cu dopant and annealing temperature on CdO_x thin films deposited on glass substrates by the spray-pyrolysis method. The Cu doping concentrations were 0, 0.46, and 1.51 at% with respect to the CdO_x undoped material. Then, the fabricated films were subjected to an annealing process at 450°C. X-ray diffraction (XRD) examination confirms that the as-deposited films show a cubic crystallographic structure with high purity of CdO in the annealed films. It was found that the (111) peak is the most predominant diffraction orientation in the surveyed samples. At the microscopic scale, the AFM machine was operated to quantify the three important parameters: the mean roughness (Ra), the root mean square value (Rq), and the z scale. These parameters hold the highest values for the sample with 0.46 at% of Cu. Finally, reflectance, absorbance, transmittance and other optical parameters from dielectric measurements were comprehensively analysed. Our evaluation of optical band gaps for the studied samples reveals that the synthesised films have a direct band gap character, as the rise in Cu content in the as-deposited films leads to a decrease in the band gap values. In contrast, annealing process results in raising the band gap.*

Keywords: *Doped: CdO_x, Spray pyrolysis, Surface morphology, Band gap, Absorption, Annealing treatment.*

1. INTRODUCTION

d-block elements have emerged as a significant class of material [1]. They found that combined structures with other gases to form oxides, nitrides, and carbides [2–4]. In particular, Cadmium oxide (CdO) compounds demonstrate an effective role in broad spectrum of transparent thermoelectric and optoelectronics applications [5–8]. CdO demonstrates cubic symmetry with a rock salt structure, has emerged as an active n-type semiconductor possessing superior characteristics, for instance, an adjustable direct bandgap of 2.2-2.7 eV [9], and high transmittance under the visible spectrum, superior electron mobility, chemical stability and tolerable electrical conductivity [10, 11]. Several cost-effective hydrothermal synthesis routes have been utilised to prepare CdO films. Most notably, the chemical bath deposition (CBD) technique [12]. The successive ionic layer adsorption and reaction (SILAR) technique was utilized to prepare pure, Mn-doped, and Mn/Cu co-doped CdO films [13]. The sonochemical route has been adopted to prepare pure and Cu-doped CdO [14]. Spray pyrolysis has been employed to fabricate pure and Pb-doped CdO [15]. The annealing treatment has always been an effective way to determine the crystallinity and stability of the films [16]. Furthermore, transition metals such as Mo and W have been introduced into the CdO lattice system by the radio frequency (RF) magnetron sputtering technique [17]. Mg-doped CdO films have been synthesised by spray pyrolysis [18]. In addition, another study reported that Sn-doped CdO could serve as a promising material for optoelectronic applications [19]. Alongside with doping strategy, annealing treatment represents an effective way to ensure phase stability [20,21]. It was reported that annealing treatment up to 550°C demonstrates the optimal temperature that results in well-crystalline CdO thin films synthesised by the sol-gel spin coating approach [22].

In the current work, pure and Cu-doped CdO thin films have been deposited by means of the spray pyrolysis approach. Cadmium chloride was used as precursor to prepare pure CdO films. The Cu-level of concentration of the deposited films was controlled by integrating a certain amount of cupric acetate at a desired weight percentage with respect to cadmium chloride. Moreover, the effect of annealing at 450°C alongside Cu-content on structural, surface morphology and optical characteristics of CdOx films was analysed

[DOI: 10.22068/ijmse.3991]

systematically.

2. EXPERIMENTAL PROCEDURES

2.1. Film' Preparations

In this work, pure and Cu-doped CdO thin films were deposited on glass substrates by spray pyrolysis method. To synthesise CdO film, cadmium nitrate tetrahydrate $Cd(NO_3)_2.4H_2O$ with a molar concentration of 0.05 M was utilised as precursor. The aqueous solution of cadmium nitrate tetrahydrate was used to prepare the precursor at room temperature by dissolving 0.1 g of cadmium nitrate tetrahydrate in 25 mL of distilled water. The solution was then stirred constantly for 30 minutes. To synthesise the source solutions of Cu, $Cu(NO_3)_2$ $3H_2O$ with a concentration of 0.05 M, the compound was dissolved in distilled water. Then, the solutions were stirred for 20 minutes.

Successive sonication baths cleaned the glass substrate in deionised water and ethanol to remove impurities. After that, the substrates were subjected to heat treatment at 400ºC with an air pressure of 1.5 bar. The distance between the boat and the glass substrate corresponds to 24 cm while the spray time lasted for 3 seconds. The number of spray cycle corresponds to 10 cycle. Lastly, the prepared samples were annealed at 450°C in air for 1 hour using a furnace type (KSL-1100 X). The samples were annealed at a fixed heating rate of 10°C min^{-1}. The annealed samples were left overnight inside the furnace after the power was turned off.

2.2. Characterization Techniques

To identify the phases present in the studied samples, X-ray diffraction (XRD) analysis must be performed. Moreover, it is of great importance to examine the chemical composition of the prepared films; therefore, Energy-dispersive X-ray (EDX) analysis was conducted to inspect the elemental composition of the studied films. Surface topography examination is performed via high-resolution atomic force microscopy (AFM) to obtain the two and three-dimensional topographical images. The AFM images are typically determined by three components at the microscopic scale, i.e., the mean roughness (Ra), rms value (Rq), and z scale. The mean roughness, Ra of an AFM image, is estimated from the following relation [23],

$$R_a = \frac{\sum_{i=1}^{N}|h_i - \bar{h}|}{N} \quad (1)$$

Where h_i represents the surface roughness value of the prepared films, $\bar{h}$ denotes the mean surface roughness, and N signifies the number of data points considered for that particular AFM image. However, root mean square (rms) is a commonly used factor to evaluate changes in surface topography. The Rq corresponds to the height deviations taken from the mean data plane and is defined as [23];

$$R_q = \sqrt{\frac{\sum_{i=1}^{N}|h_i - \bar{h}|^2}{N}} \quad (2)$$

The films' thicknesses must be initially obtained when calculating optical properties. For this reason, a Scanning Electron Microscope (SEM) test has been conducted to obtain cross-sectional images, allowing the display of thickness at different locations. Finally, the Ultraviolet-visible (UV-vis) machine was utilised to obtain the absorbance and transmittance spectra, from which all the optical characteristics and dispersion parameters of the inspected films can be calculated.

3. RESULTS AND DISCUSSION

3.1. Structural Properties Analysis and Elemental Composition Examinations

XRD patterns of the Cu-doped CdO_x films before and after being annealed at 450°C are pictured in Figures 1 and 2. XRD analysis of as-deposited films at different molar concentrations of Cu precursor solutions. Figure 1 demonstrates that there are three prominent peaks belonging to cubic-structured CdO (a=b=c= 4.69 Å) with a space group of Fm-3m [24]. This result aligns well with the (ICDD) card no. (75-0592) [25]. The peaks are (111), (200) and (220) oriented at (2θ) of 33.01°, 38.30° and 55.28°, respectively. Moreover, Figure 1 displays several predominant peaks below 30°. These peaks could be assigned to tetragonal $Cd(OH)_2$, which may be formed during the preparation process [26]. The general consensus of literature results confirms that the annealing procedure would confidently enhance the decomposition of $Cd(OH)_2$ entities and thereafter develop thin film coatings with high purity of CdO_x [26, 27]. For this reason, annealing treatment at 450°C was adopted to derive pure CdO films. As shown in Figure 2, the peaks below 30° disappear, resulting in an increase in the peak

[DOI: 10.22068/ijmse.3991]

intensities of CdO. It is remarkable to note that the dominant peak of our measured CdO films corresponds to a (111) orientation, indicating highly preferable films with a very low surface energy, as these film coatings possess high atomic packing densities. The information obtained from the XRD peaks can be utilised as inputs to calculate the crystallite size (D) by applying the Scherrer equation as expressed below [28],

$$D = \frac{K\lambda}{\beta(\theta)\cos(\theta)} \quad (3)$$

in which K signifies a constant amounted to 0.94, λ refers to the wavelength of Cu-Ka radiation used in XRD instrument, which corresponds to 0.1541 nm, β(θ) denotes the full width at half maximum in radians, and θ indicates the angle of the most intense peak in XRD. Table 1 records D values of the studied films. From the table, it can be observed that the crystallite size decreases as Cu content rises, whereas the crystallite size of the films exhibits an annealing-dependent increase. This trend could be attributed to eliminating crystal defects and improving the crystallinity degree [29]. Energy-dispersive X-ray (EDX or EDS) is an analytical technique that supplies adequate information about the chemical composition of a compound material. Figures 3-8 elucidate EDS plots and elements' maps of the scanned area of pre and post-annealed films. It is worth mentioning that the microstructure images of the entire examined area and of each component are displayed individually in the figures. The plots were analysed to report the atomic percent of the films as listed in Table 1. As can be seen from the table, Cu atomic percentages in the as-deposited doped films are (0, 0.46, and 1.51) at% which are labelled as S1, S2 and S3. For the corresponding annealed samples, they are labelled as SA1, SA2 and SA3.

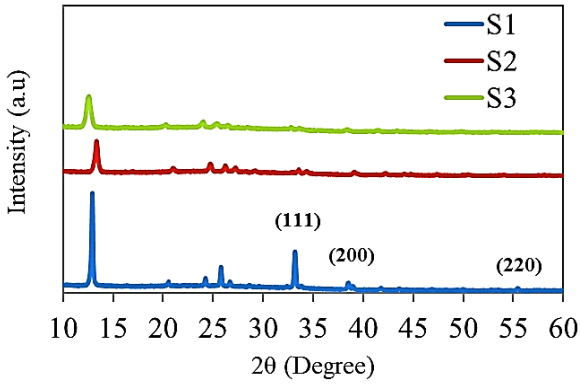

Fig. 1. XRD patterns for the as-deposited samples. S1, S2 and S3 resemble pure, 0.46 at%, and 1.51 at%, respectively

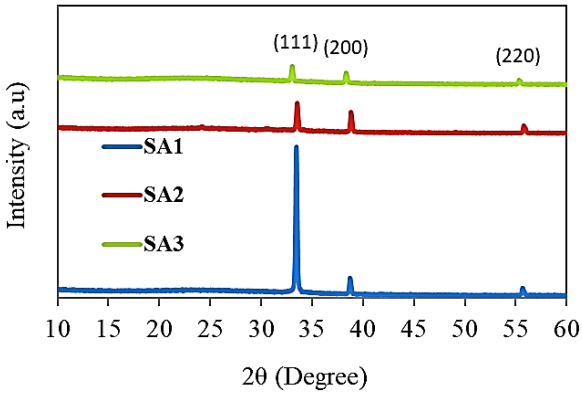

Fig. 2. XRD patterns for the annealed samples. SA1, SA2 and SA3 correspond to pure, 0.46 at%, and 1.51 at%, respectively

Table 1. The structural properties results of the prepared samples

Sample Code	Atomic % of Cd	Atomic % of Cu	Atomic % of O	Crystallite Size (nm)	Film Thickness (nm)
S1	6.9	-	93.1	43.97	104.4
SA1	16.9	-	83.1	45.62	765.1
S2	14.77	0.46	84.60	21.42	166.5
SA2	25.71	1.25	72.99	46.11	181.1
S3	8.33	1.51	90.15	15.76	202.6
SA3	11.02	1.74	87.22	48.46	190.1

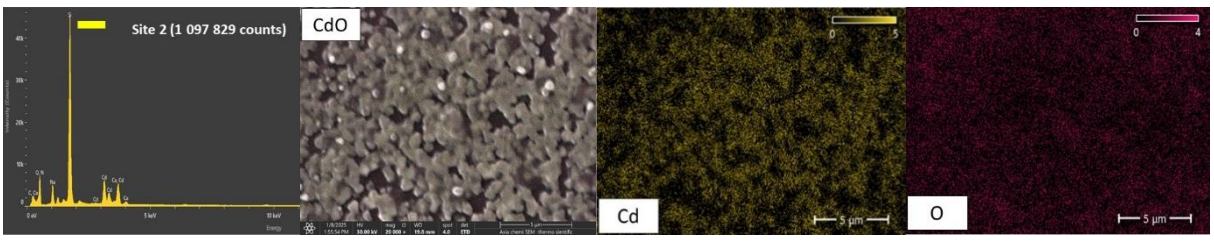

Fig. 3. EDS images showing elements' distribution maps of the as-prepared pure CdO film (S1)

[DOI: 10.22068/ijmse.3991]

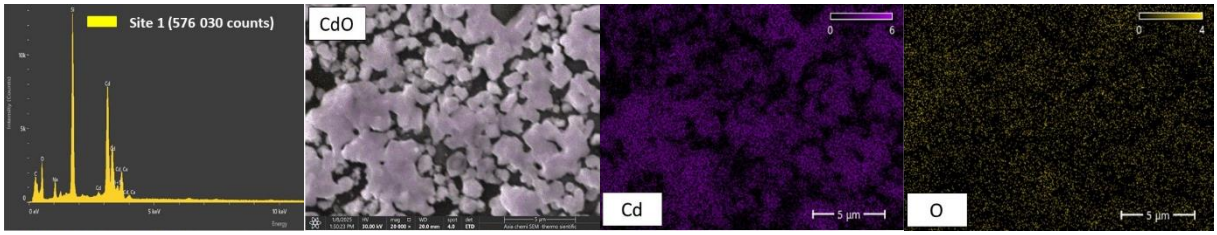

Fig. 4. EDS images viewing elements distribution maps of the annealed CdO film (SA1)

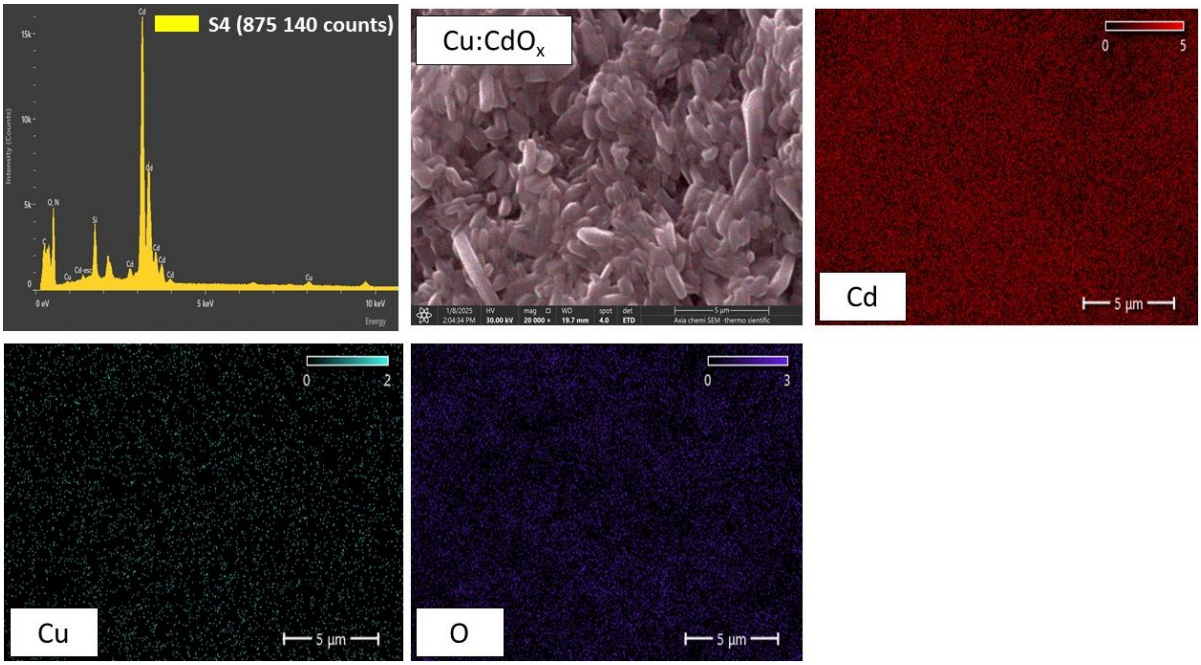

Fig. 5. EDS images displaying the element distribution maps of the as-prepared Cu: CdO_x film (S2). Where x corresponds to 0.45 at%

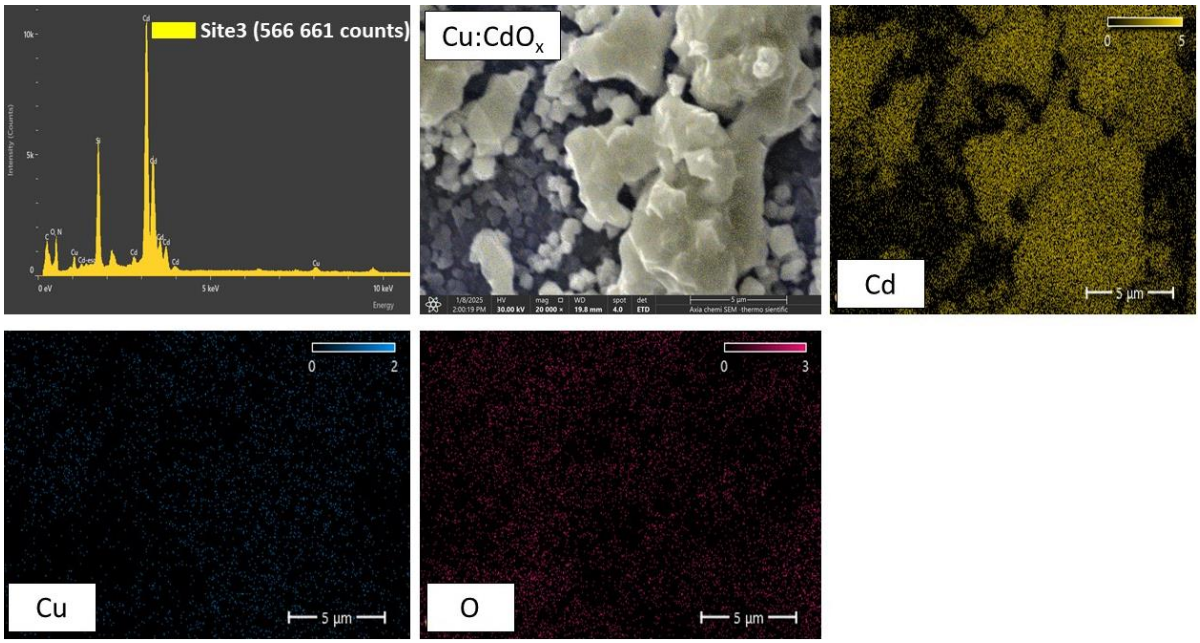

Fig. 6. EDS images showing the distribution maps of the post-deposited Cu: CdO_x film (SA2).Where x corresponds to 0.45 at%

[DOI: 10.22068/ijmse.3991]

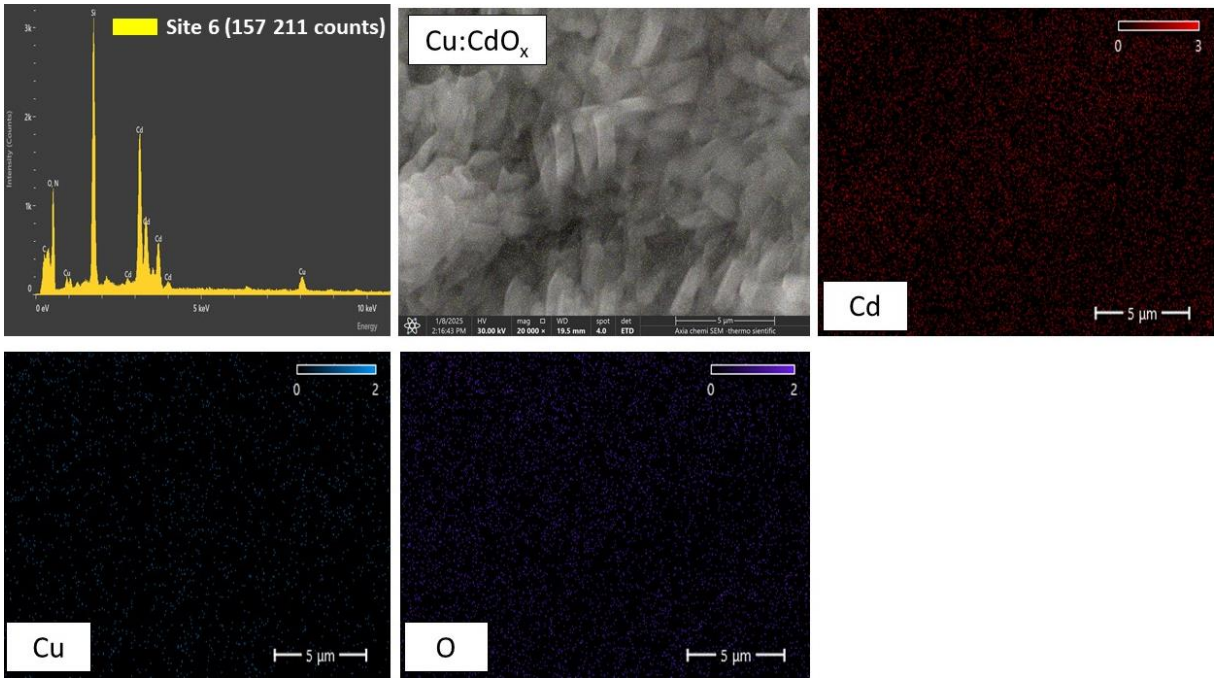

Fig. 7. EDS images displaying the element distribution maps of the as-prepared Cu: CdO_x film (S3). Where x corresponds to 1.51 at%

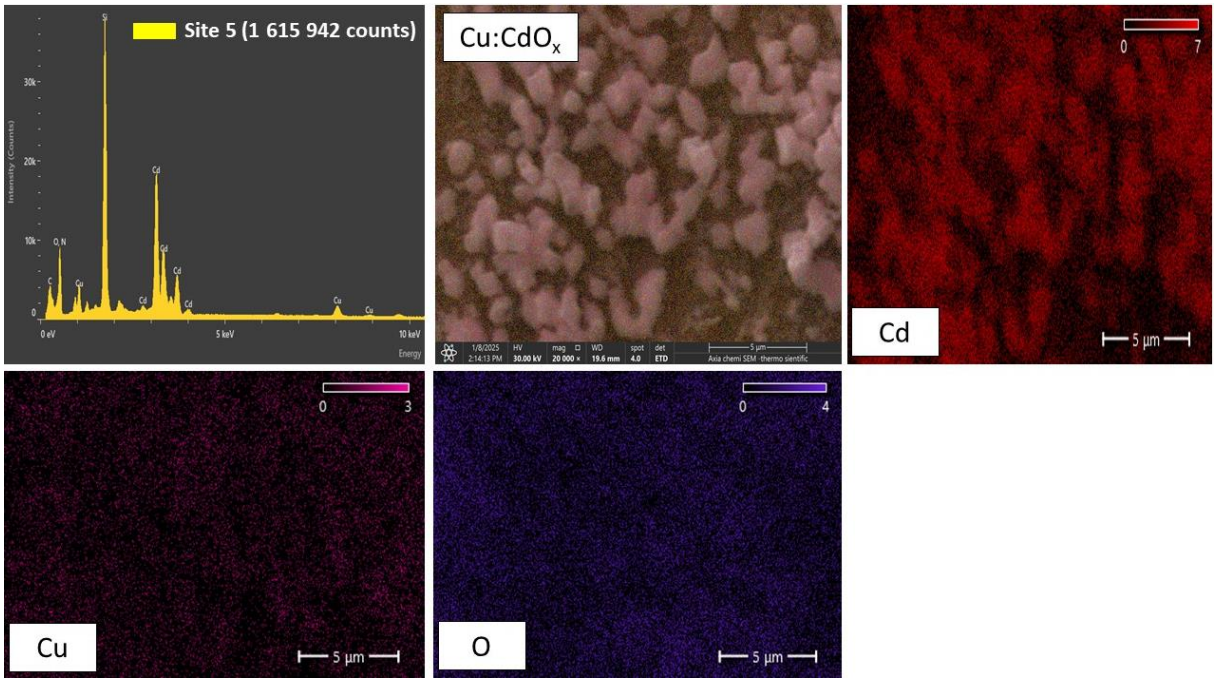

Fig. 8. EDS images illustrating the distribution maps of the post-deposited Cu: CdO_x film (SA3).Where x corresponds to 1.51 at%

3.2. Surface Topography Measurements

The surface topographies of the pure and Cu-doped CdOx films, before and after annealing, as observed by the AFM machine, are depicted in Figure 9. The three scaled-microscopic parameters of the mean roughness (Ra), root-mean-square value (Rq), and z-scale images, quantified by AFM, were estimated and listed in Table 2. The mean roughness (Ra) and rms (Rq) values of the Cu-CdO_x films before annealing are observed to be less than those of the annealed films. Both Ra and Rq of the assessed films were potentially

[DOI: 10.22068/ijmse.3991]

enhanced after annealing at 450°C, with an average image surface area of 1.569 μm^2. This finding suggests that the annealing process has a positive influence on the surface topographical characteristics of Cu-CdO_x films. Literature attributes the positive influence of annealing to the significant grain growth that occurs around the film surface [30].

It is noticeable that the mean roughness (Ra) and rms value (Rq) increase as the Cu content rises. From the crystallite sizes (displayed in Table 1) and the mean roughness, Ra and rms values, Rq (shown in Table 2), it can be inferred that our prepared samples and their corresponding annealed ones have nanostructured configurations. Scanning electron microscopy (SEM) was used to obtain cross-sectional images, as shown in Figure 10. In fact, different cross-sectional spots on the films have been chosen to compute the average thicknesses. This is achieved, as it is a typical step in any experimental work aimed at surveying the optical properties of a material. The thicknesses of our films are disclosed in Table 1.

3.3. Optical Response Investigations

The ability of a substance to collect and absorb sunlight can be assessed by its absorption coefficient (α) [31, 32]. At variant Cu ratios, the absorbance and transmittance spectra in the ultraviolet and visible range have been attained using a UV-Vis instrument.

Table 2. Surface characteristics of pure and Cu-doped CdO as a function of annealing temperature

Sample Code	Mean Roughness, Ra (nm)	rms Value of the Surface Roughness, Rq (nm)	z Scale (nm)	Image Surface Area (μm)^2	Band Gap Energy (eV)
S1	7.8412	9.4163	88.7	1.569	3.81
SA1	39.101	46.005	188.5	1.569	3.85
S2	15.215	18.177	274.0	1.569	3.72
SA2	68.408	84.308	376.0	1.569	3.73
S3	19.89	26.049	174.9	1.569	3.65
SA3	43.491	51.447	381.0	1.569	3.74

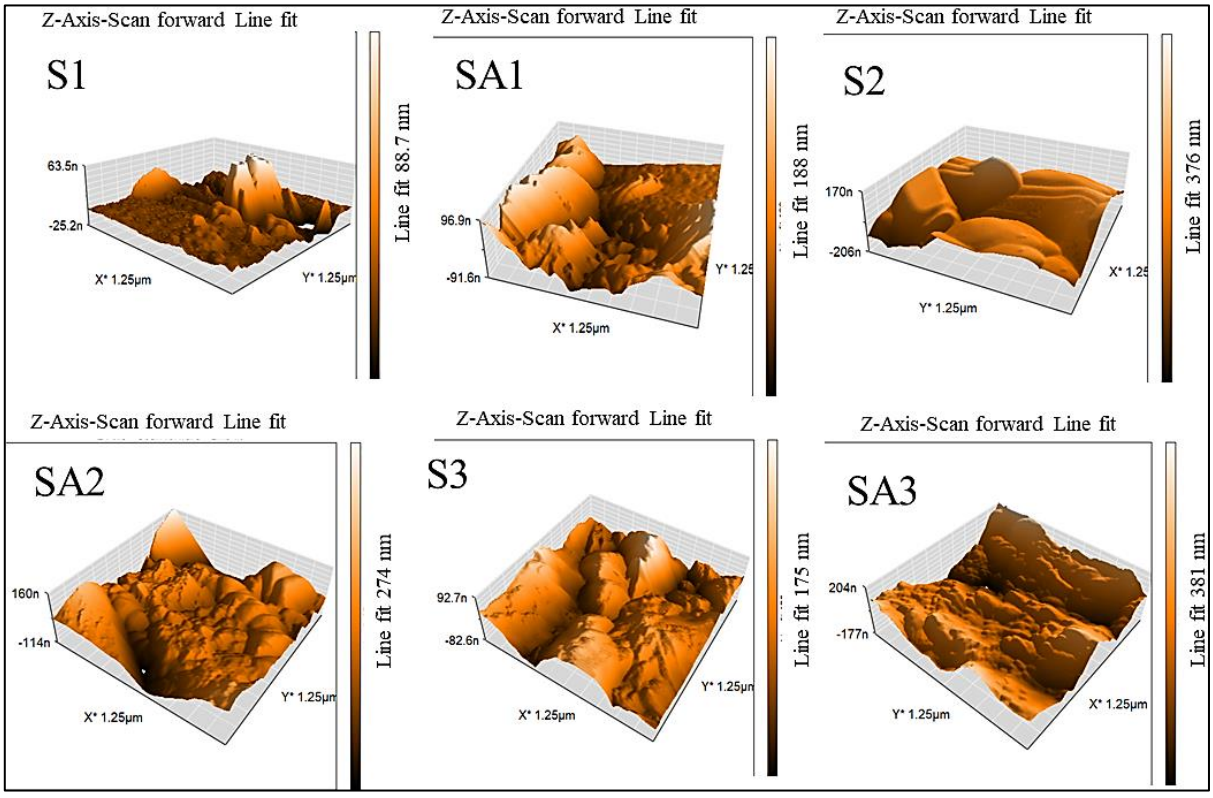

Fig. 9. Three-dimensional AFM images for pure and Cu doped CdO_x samples deposited at room temperature and annealed at 450□

[DOI: 10.22068/ijmse.3991]

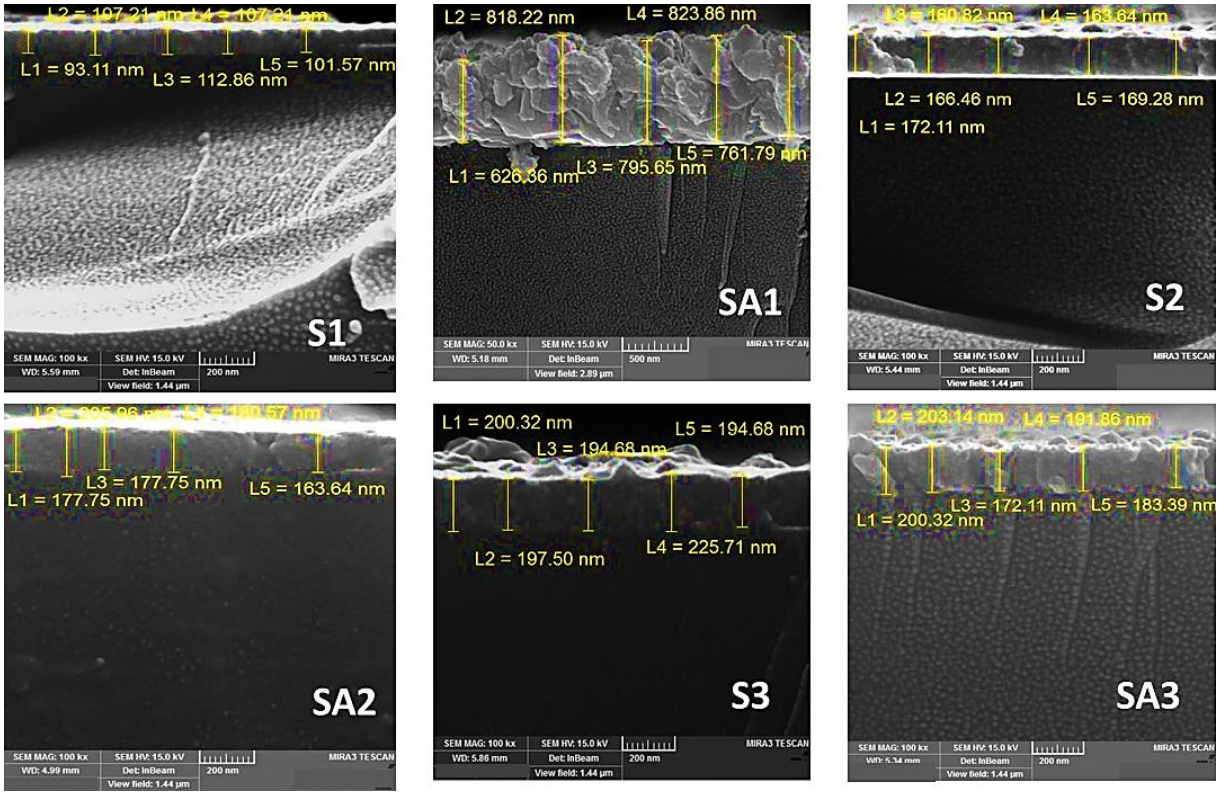

Fig. 10. SEM cross-section images for the as-deposited and post-annealed films grown by the spray pyrolysis method

As illustrated in Figure 11, the values of the absorption coefficient for all prepared films were found to be ($\alpha > 10^4$ cm^{-1}), signifying direct allowed transitions for the visible region.

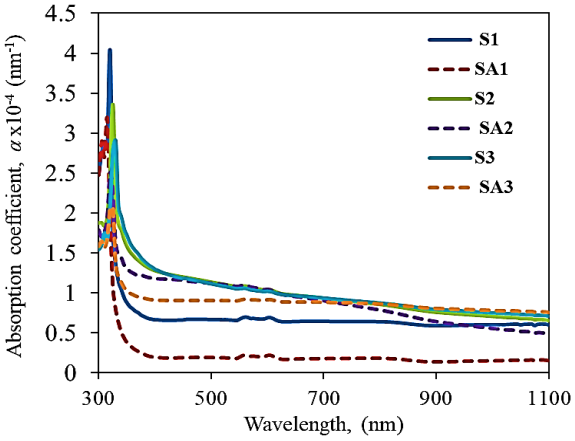

Fig. 11. Absorption coefficient profile for the as-deposited and annealed pure and Cu-doped CdO films

Furthermore, the figure displays that the absorbance spectra (A) have been improved with increasing Cu-doping concentration in the visible range.
At higher Cu-loadings, the films demonstrate an enhancement in terms of their capability toward absorbing solar incident photons, while revealing a transparency-decreasing behaviour. The annealed Cu-loaded films exhibit slight changes in their absorbance and transmittance curves compared to the corresponding as-deposited ones. The absorbance and the transmittance data collected from the UV-Vis instrument have been used to calculate the reflectance of the films using the following formalism;

$$A + T + R = 1 \quad (4)$$

Where A, T and R correspond to absorbance, transmittance and reflectance of the incident solar radiation, respectively.
The direct optical energy gap (E_g) of as-synthesized and post-annealed CdO_x has been surveyed utilizing the optical absorption coefficient spectra and using the formula proposed by Tauc, according to the equation below [33],

$$\alpha E = A\left(hv - E_g\right)^n \quad (5)$$

Where E refers to the photon energy (hv) h represents Planck's constant, v stands for the fallen photons' frequency, A denotes the probability factor of the optical transition, E_g symbolizes the optical band-gap energy, and n may occupy various

[DOI: 10.22068/ijmse.3991]

values based on the kind of electronic transition. Herein, n=2 or 1/2 permits the occurrence of indirect or direct optical transitions, correspondingly. The direct band-gap is calculated by plotting E verses $(\alpha E)^2$ and extrapolating the linear portion of the spectrum to the value of $(\alpha E)^2$ being equal to zero in the X-axis. Similarly, the indirect band gap is calculated via plotting E against $(\alpha E)^{1/2}$ and inferring the linear portion of the spectrum to $(\alpha E)^{1/2}$ value is equal to along the X-axis. Figure 12 manifests the plots of $(\alpha E)^2$ versus fallen photon energy (E) of as-deposited and post-annealed pure and Cu-included CdO_x systems. As seen from the figure, the direct optical band-gap of the starch coatings ranges from nearly 3.85 to 3.65 eV. It is noteworthy to mention that introducing dopants of smaller ionic radii compared with Cd ensures relaxation of oxide anions around cation dopants, resulting in weaker hybridisation between Cd and O. In addition, the shrinkage of lattice parameters has affected in narrowing the band gap [34].

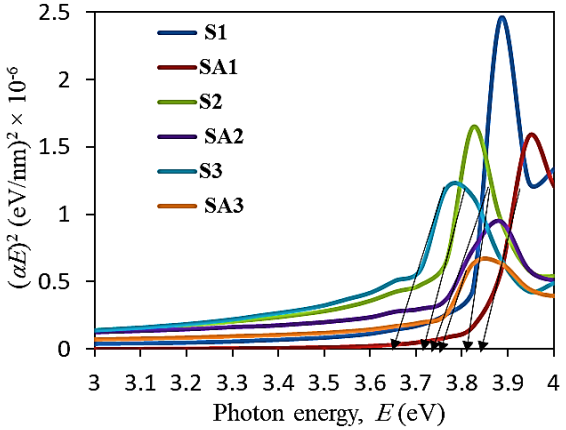

Fig. 12. Tauc plots of optical band gap energy $(\alpha E)^2$ as a function of photon energy of the studied films

Implying that with increasing Cu contents, the band-gap energy values of the synthesised films are diminished. In contrast, temperature annealing at 450°C increased the band-gap for the corresponding films. The absorbance data of the prepared films is utilized to obtain the absorption coefficient profile of the prepared samples. The absorption coefficient (α) of the six samples of Cu-CdO_x films has been calculated by the following relation [35],

$$\alpha = 2.3\frac{A}{d} \quad (6)$$

A and d symbolise the absorbance data derived from UV-vis experimentation and the thickness of the tested films, respectively. Figure 13 shows the solar photon wavelength dependence of the absorption coefficient (α) of spray pyrolysis-derived Cu: CdO_x films prior to and after annealing. Introducing the Cu element into the host CdO_x system has a positive influence on the α value in the UV and visible range of electromagnetic wavelengths. On the other side, the annealing process has not influenced the improvement of α values.

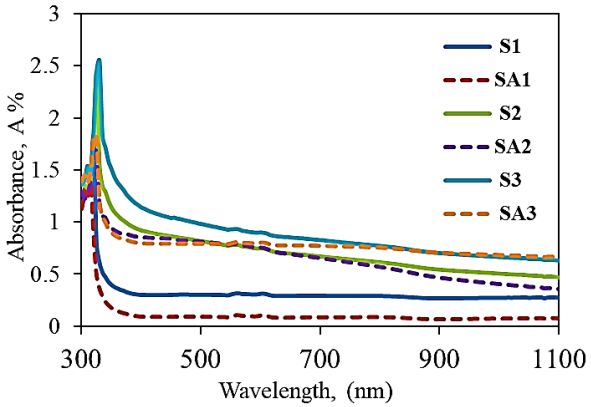

Fig. 13. Absorbance profile dependent wavelength for the considered samples with and without heat treatment

As can be pictured in Figure 14, for pure CdO film, namely, (S1 sample), it was indicated that at approximately 400 nm wavelength, the value of transmittance (T) corresponds to approximately 50%. However, for the rest of the samples, there is a significant shrinkage in the transparency trend at higher Cu loading levels. Interestingly, this finding motivates the research to look further into the absorption spectra of the considered films.

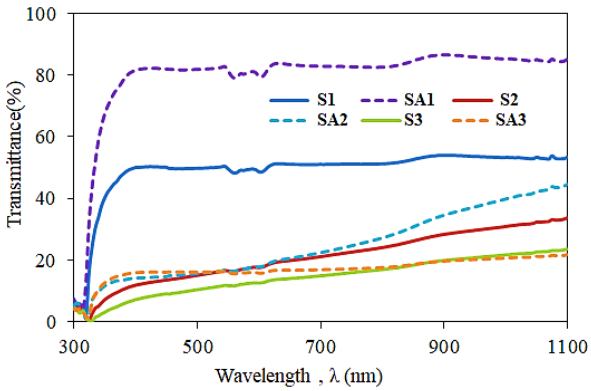

Fig. 14. Transmittance spectra as a function of photon wavelength for the considered samples

From Figure 15, it can be observed that pure annealed CdO_x and the film loaded with Cu at

[DOI: 10.22068/ijmse.3991]

0.46 at% (i.e., SA1 and SA2) exhibit high anti-reflection performance in the visible region, motivating the use of these materials in solar cell technologies. This is ascribed to our obtained findings of Ra and Rq values (see Table 2) that revealed elevated values referring to occurring further scattering process of the incident solar radiations, and this is in line with what has been reported in the literature. Additionally, the sample labelled SA3 showed high reflectance character despite its high surface reflectance, and this may be due to introducing a greater content of Cu element into the host compound, as revealed in Figure 10.

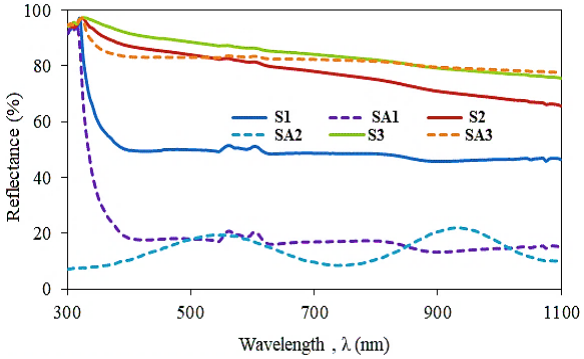

Fig. 15. Reflectance spectra versus photon wavelength for the study samples

3.4. Optical Dispersion and Dielectric Analysis

Reflectance results computed by the absorbance and transmittance data derived from the UV-vis instrument can be directly used to obtain dispersion constants such as refractive index (n) and extinction coefficient (k). The complex refractive index is expressed as below [36],

$$n^* = n + ik \quad (7)$$

Where n corresponds to the real part (refractive index), whereas k represents the imaginary part that is a measure of how much energy is absorbed or dissipated in the material. k value can be expressed according to the following relation [35],

$$k = \frac{\alpha\lambda}{4\pi} \quad (8)$$

Where α denotes the absorption coefficient and λ symbolises the incident photon wavelength. As mentioned earlier, the computed reflectance data are employed to obtain the refractive index n through the expression below [35],

$$n = \left(\frac{1+R}{1-R}\right) + \sqrt{\frac{4R}{(1-R)^2} - k^2} \quad (9)$$

Figure 16(a) shows the refractive index (n) values versus the incident photon wavelength of the inspected thin films. From the figure, it can be observed that the rise in Cu concentrations enhances the dispersion character in the visible area of the electromagnetic spectrum, while the annealing process has no evident impact on the improvement of the refractive index of the studied films.

The extinction coefficient (k)–wavelength dependency plot displayed in Figure 16(b) reveals that our studied films have relatively higher values in the ultraviolet and visible regions for those samples with higher Cu content. This finding confirms our results on the absorbance data. The correlation between frequency-dependent dielectric functions with refractive index and extinction coefficient is expressed by the momentum matrix elements between occupied and unoccupied states, as expressed below [35],

$$\varepsilon(\omega) = \varepsilon_1(\omega) + i\varepsilon_2(\omega) = \left(n(\omega) + ik(\omega)\right)^2 \quad (10)$$

Where $\varepsilon_1(\omega)$ and $\varepsilon_2(\omega)$ represent the real part and imaginary part of the complex dielectric function, respectively, that can be calculated by the following formalisms.

$$\varepsilon_1 = n - k \text{ and } \varepsilon_2 = 2nk \quad (11)$$

The real and imaginary portions of the complex dielectric functions as a function of the photons' wavelengths are pictured in Figure 17(a-b). The same trend as for refractive indices has been observed in the dielectric results.

The annealing temperature does not have a clear influence on Cu-loaded systems. On the one hand, an enhancement has been observed with samples of higher Cu dopants in the visible and UV ranges of interest. This enhancement in dielectric constants, in turn, leads this material to be employed in dielectric device applications such as capacitor industries.

Furthermore, the films exhibit a trivial dielectric character in this frequency region, which is attributed to the increase in electron density of the thin films. The findings on the surface roughness of the film coatings validate the imaginary dielectric results, indicating absorption as a result of the scattering process. Charge transfer and charge conduction processes occur as a consequence of the inelastic scattering interaction, leading to power loss. This energy loss can be quantified as the loss tangent, that expressed as [35],

$$\tan\delta = \frac{\varepsilon_2}{\varepsilon_1} \quad (12)$$

[DOI: 10.22068/ijmse.3991]

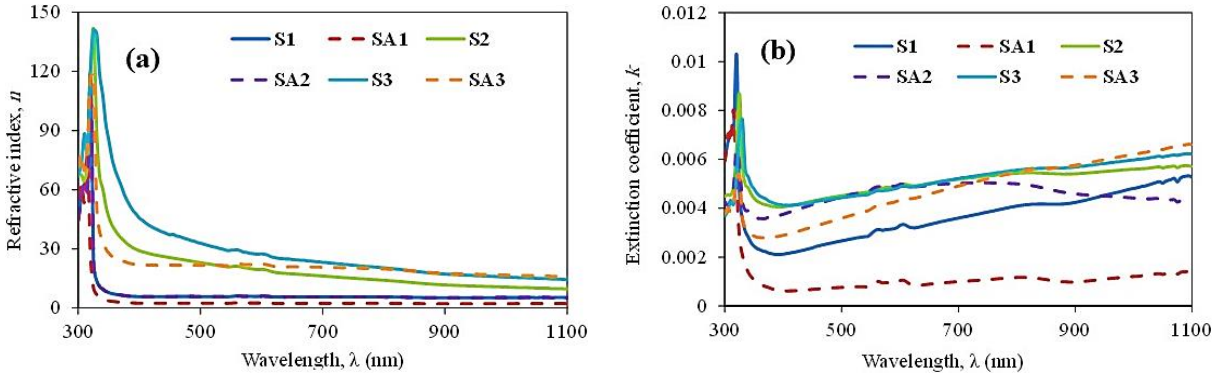

Fig. 16. a) Refractive index and b) extinction coefficient as a function of photon wavelength for the study samples

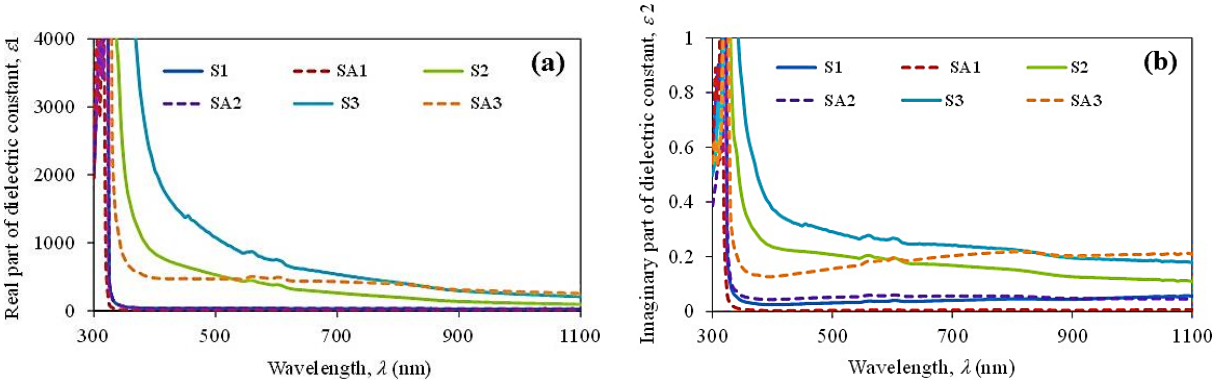

Fig. 17. a) Real components and b) Imaginary components of dielectric constant as a function of photon wavelength for the prepared films

Figure 18 plots the loss tangent values of CdO_x films fabricated at variant Cu concentrations as a function of the incident wavelength. It is evident from the figure that the loss tangent indicates that the entire fabricated thin film reveals trivial quantities of energy loss.

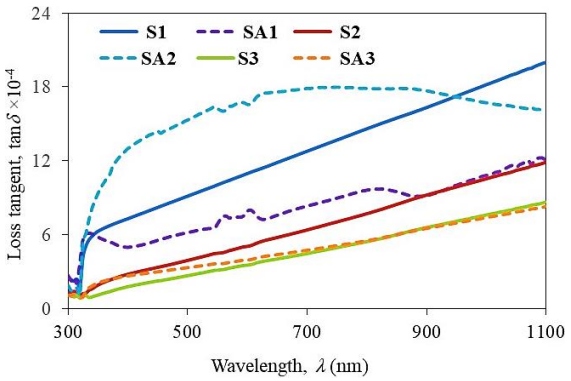

Fig. 18. Loss tangent versus photon wavelength for the prepared films

Ultimately, the volume energy loss function (V_{el}) expresses the optical transitions for electrons in the bulk compound, while the surface energy loss function (Sel) delineates the electron transition of a material in the form of the thin film.The volume and surface energy loss functions of the fabricated films were assessed according to the following equations [37].

$$V_{el} = \frac{\varepsilon_2}{\varepsilon_1^2+\varepsilon_2^2} \quad (13)$$

$$S_{el} = \frac{\varepsilon_2}{(\varepsilon_1+1)^2+\varepsilon_2^2} \quad (14)$$

The bulk and surface loss schemes as a function of photon wavelength are revealed in Figure 19(a-b). Varying bulk and surface energy loss trends can be interpreted as a result of changes in the electron transition energy.

4. CONCLUSIONS

In this work, CdO and various molar concentrations of Cu-doped CdO_x films have been fabricated by the spray pyrolysis route and deposited over glass substrates. The films were exposed to annealing treatment at 450°C. X-ray diffraction profiles display that the synthesized films exhibit poly-crystalline. The structural characterisation analysis confirms that the films crystallise in a cubic structure.

[DOI: 10.22068/ijmse.3991]

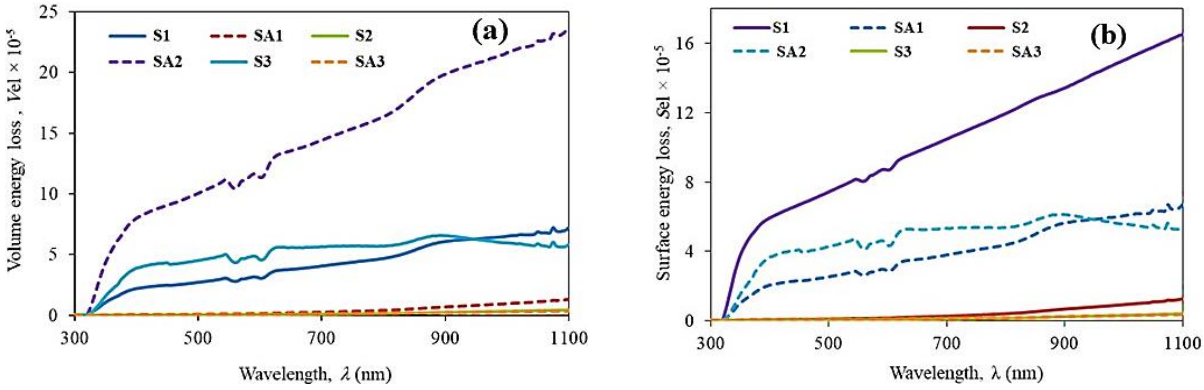

Fig. 19. a) Volume energy loss and b) surface energy loss for the prepared films

Increasing the Cu molarity produced an increase in film crystallinity. Crystallite size calculations reveal a decrease in the crystallite size as Cu is introduced into the host system, whereas the annealing process results in an increase in the crystallite sizes of the films. When the molar concentrations of Cu increase, the optical band gap values diminish from 3.85 to 3.65 eV. The SEM analysis confirms the presence of Cd and O in the as-deposited and Cd, Cu, and O in the Cu-doped films. Furthermore, the results demonstrate an improvement in the band gap with increasing annealing temperature. Optical characteristics were inspected at photon wavelengths extended from 300 to 1100 nm. Introducing Cu contents into the host system has stretched the absorption property of the material to cover the visible range. Moreover, it is observed that the energy loss behaviour of the studied films exhibits minor magnitudes in the visible range. Consequently, these compounds hold great significance in optoelectronics and energy harvesting applications.

REFERENCES

[1] Edwin C. Constable, "Evolution and Understanding of the D-Block Elements in the Periodic Table" Dalton Trans., 2019, 48, 9408-9421. https://doi.org/10.1039/C9DT00765B.

[2] Navajsharif S. Shaikh, Shivaji B. Ubale, Vikas J. Mane, Jasmin. S. Shaikh, Vaibhav. C. Lokhande, Supareak Praserthdam, Chandrakant D. Lokhande, Pongsakorn Kanjanaboos "Novel Electrodes for Supercapacitor: Conducting Polymers, Metal Oxides, Chalcogenides, Carbides, Nitrides, MXenes, and their Composites with Graphene" J.Alloys Compd., 2022, 893, 161998. https://doi.org/10.1016/j.jallcom.2021.161998.

[3] Hussein A. Miran, Zainab N. Jaf, Imad H. Khaleel, Abdulkareem A. Alkhafaji "Photocatalytic and Optical Performances of CeO_2 by Substitution of Titanium" Phys. Chem. Res., 2021 9, 553,. https://doi.org/10.22036/pcr.2021.270358.1878.

[4] Zainab N Jaf, Mohammednoor Altarawneh, Hussein A Miran, Zhong-Tao Jiang "Geometries, Electronic Properties and Stability of Molybdenum and Tungsten Nitrides Low-Index Surfaces" Mater. Res. Express, 2018, 5, 126402. https://doi.org/10.1088/2053-1591/aadeb6.

[5] Ahmed A. Aboud, Ayan Mukherjee, Neerish Revaprasadu, Ahmed Nagaty Mohamed "The Effect of Cu-Doping on CdS Thin Films Deposited by the Spray Pyrolysis Technique" J. Mater. Res. Technol., 2019, 8, 2021. https://doi.org/10.1016/j.jmrt.2018.10.017.

[6] Ali Badawi, M.G. Althobaiti,Sami S. Alharthi, Ateyyah M. Al-Baradi "Tailoring the Optical Properties of CdO Nanostructures via Barium Doping for Optical Windows Applications" Phys. Lett. Sect. A Gen. At. Solid State Phys. 2021, 411, 127553. https://doi.org/10.1016/j.physleta.2021.127553.

[7] X. K. Ning, W. B. Guo, J. Y. Han, Y. M. Ran, W. X. Jian, X. Y. San, L. J. Gao, S. F. Wan "CdO: A Promising Flexible and Transparent Thermoelectric Power Generator" Appl. Phys. Lett. 2025, 126. https://doi.org/10.1063/5.0249540.

[8] Zain A. Muhammad, Ahmed T. Hassan,

[DOI: 10.22068/ijmse.3991]

Yasmeen Z. Dawood "Studying the Optical Properties of CdO and CdO: Bi Thin Films", Baghdad Sci. J. 2016, 13, 0593. https://doi.org/10.21123/bsj.2016.13.3.0593.

[9] B. Amudhavalli, R. Mariappan, M. Prasath "Synthesis Chemical Methods for Deposition of ZnO, CdO and CdZnO Thin Films to Facilitate Further Research, J. Alloys Compd. 2022, 925, 166511. https://doi.org/10.1016/j.jallcom.2022.166511.

[10] Mauricio Ortega, Guillermo Santana, Arturo Morales-Acevedo "Optoelectronic Properties of CdO/Si Photodetectors" Solid. State. Electron. 2000, 44, 1765. https://doi.org/10.1016/S0038-1101(00)00123-4.

[11] Hakan Çolak, Orhan Türkoğlu "Structural and Electrical Studies of Cu-Doped CdO Prepared by Solid State Reaction" Mater. Sci. Semicond. Process. 2013, 16, 712. https://doi.org/10.1016/j.mssp.2012.12.013.

[12] R. Nallendran, G. Selvan, A.R. Balu "CdO-Fe_3O_4 Nanocomposite with Enhanced Magnetic and Photocatalytic Properties" Mater. Sci. Pol. 2019, 37, 100. https://doi.org/10.2478/msp-2019-0012.

[13] R. Aydin, H. Cavusoglu, B. Sahin "Transition Metal Mn/Cu Co-Doped CdO Transparent Conductive Films: Effect on Structural, Morphological and Optical Characteristics" J. Alloys Compd. 2019, 785, 523. https://doi.org/10.1016/j.jallcom.2019.01.221.

[14] Abdollah Eskandari, Farid Jamali-Sheini "Sonochemical Synthesis of Cu-Doped CdO Nanostructures and Investigation of Their Physical Properties" Mater. Sci. Semicond. Process. 2018,74, 210. https://doi.org/10.1016/j.mssp.2017.08.028.

[15] Harun Güney, The Structural, Morphological, Optical and Electrical Properties of Pb Doped CdO Thin Films Grown by Spray Method" Vacuum. 2019, 159, 261. https://doi.org/10.1016/j.vacuum.2018.10.053.

[16] M. Azizar Rahman, M.K.R. Khan "Effect of Annealing Temperature on Structural, Electrical and Optical Properties of Spray Pyrolytic Nanocrystalline CdO Thin Films" Mater. Sci. Semicond. Process. 2014, 24, 26. https://doi.org/10.1016/j.mssp.2014.03.002.

[17] Ying Wang, Yuen Yan Chow, Cheuk Kai Gary Kwok,Yau Fung Leung, Kin Man Yu "Effects of Transition Metal Dopants (Mo and W) on Electrical and Optical Properties of CdO Thin Films" J. Alloys Compd. 2023, 935, 168116. https://doi.org/10.1016/j.jallcom.2022.168116.

[18] K. Usharani, A.R. Balu, V.S. Nagarethinam, M. Suganya "Characteristic Analysis on the Physical Properties of Nanostructured Mg-Doped CdO Thin Films-Doping Concentration Effect" Prog. Nat. Sci. Mater. Int. 2015, 25, 251. https://doi.org/10.1016/j.pnsc.2015.06.003.

[19] V. Saravanan, M. Anusuya, Cyril O. Ugwuoke, Nnamdi Nwulu, Fabian I. Ezema "Structural, Electrical and Nonlinear Optical Characterization of Sn-Doped CdO Thin Film Synthesized via Spray Pyrolysis for Optoelectronic Applications" Results Opt.2023, 13, 100548. https://doi.org/10.1016/j.rio.2023.100548.

[20] N.-A. Hassan, Zainab N. Jaf, Seham Hassan Salman, Iman Hameed Khudayer, Hanaa Ibrahem, Hussein A. Miran "Influence of In-Dopant on the Optoelectronic Properties of Thermal Evaporated $CuAlTe_2$ Films" Solid State Commun. 2023, 371, 115260. https://doi.org/10.1016/j.ssc.2023.115260.

[21] Yong Ma, Chen Zhang, Dingkun Shi, Dongsheng Chen, Xiaojing Luo, Tatiana Dyachkova, Alexander Tyutyunnik, Vladimir Krasil'nikov, Vyacheslav V.Marchenkov, Yuriy Dedkov, Yefei Guo, Tian Gao "Structural and Magnetic Properties of Cadmium Oxides with Different Annealing Temperatures" J. Alloys Compd. 2024, 998, 174988. https://doi.org/10.1016/j.jallcom.2024.174988.

[22] Aziz Nfissi, Mounir Belhajji, Abdelhak Chouiekh, Abdelilah Rjeb, Abdelfettah Barhdadi, Salaheddine Sayouri, Yahya Ababou "Investigation of the Structural, Electrical and Optical Properties of Zr-Doped CdO Thin Films for Optoelectronic Applications" J. Sol-Gel Sci. Technol. 2023, 108, 401. https://doi.org/10.1007/s10971-023-06194-8.

[23] Maria Raposo, Quirina Ferreira, Paulo Ribeiro "A Guide for Atomic Force Microscopy Analysis of Soft- Condensed Matter, Modern research and educational

[DOI: 10.22068/ijmse.3991]

topics in microscopy" 2007. https://api.semanticscholar.org/CorpusID:14444095.
[24] Islem Ben Miled, Mohamed Jlassi, I. STA, Mehdi Dhaouadi "Structural, Optical, and Electrical Properties of Cadmium Oxide Thin Films Prepared by Sol–Gel Spin-Coating Method" J. Sol-Gel Sci. Technol. 2017, 83, 259. https://doi.org/10.1007/s10971-017-4412-1.
[25] Abd. F. Haneen, Khodair T. Ziad, Gailan Asad Aldainy "Structural and Optoelectronic Properties of Nickel Doped CdO Thin Films Deposited by Spray Pyrolytic Technique" Nexo Rev. Científica. 2023, 36, 1062. https://doi.org/10.5377/nexo.v36i06.17463.
[26] M Ristić, S Popović, S Musić "Formation and Properties of $Cd(OH)_2$ and CdO Particles" Mater. Lett. 2004, 58, 2494. https://doi.org/10.1016/j.matlet.2004.03.016.
[27] Duha M.A. Latif, Ikhlas H. Shallal, Aliyah A. Shuihab "Synthesis and Properties of Cadmium Oxide Thin Films Prepared by Simple Chemical Method" Energy Procedia, 2019, 157, 261. https://doi.org/10.1016/j.egypro.2018.11.189.
[28] Ahmad Monshi, Mohammad Reza Foroughi, Mohammad Reza Monshi "Modified Scherrer Equation to Estimate More Accurately Nano-Crystallite Size Using XRD" World J. Nano Sci. Eng. 2012, 02, 154. https://doi.org/10.4236/wjnse.2012.23020.
[29] Yuhan Li, Ziteng Ren, Zhengjiang He, Ping Ouyang, Youyu Duan, Wendong Zhang, Kangle Lv, Fan Dong "Crystallinity-Defect Matching Relationship of g-C_3N_4: Experimental and Theoretical Perspectives" Green Energy and Environment. 2024, 9, 623-658. https://doi.org/10.1016/j.gee.2023.02.012.
[30] Hussein A. Miran, M. Mahbubur Rahman, Zhong-Tao Jiang, Mohmmednoor Altarawneh, Lee Siang Chuah, Hooi-Ling Lee, Ehsan Mohammedpur, Amun Amri, Nicholas Mondinos, Bogdan Z. Dlugogorski "Structural and Optical Characteristics of Pre- and Post-Annealed Sol-Gel Derived CoCu-Oxide Coatings" J. Alloys Compd. 2017, 701, 222. https://doi.org/10.1016/j.jallcom.2017.01.079.
[31] Hussein A. Miran, Zainab N. Jaf "Electronic and Optical Properties of Nickel-Doped Ceria: A Computational Modelling Study" Pap. Phys. 2022, 14, 140002. https://doi.org/10.4279/pip.140002.
[32] Hussein A. Miran, Mohammednoor Altarawneh, Hantarto Widjaja, Zainab N. Jaf, M. Mahbubur Rahman, Jean-Pierre Veder, Bogdan Z. Dlugogorski, Zhong-Tao Jiang "Thermo-Mechanical Properties of Cubic Lanthanide Oxides" Thin Solid Films. 2018, 653, 37. https://doi.org/10.1016/j.tsf.2018.01.063.
[33] J. Tauc, R. Grigorovici, A. Vancu "Optical Properties and Electronic Structure of Amorphous Germanium", Phys. Status Solidi. 1966, 15, 627. https://doi.org/10.1002/pssb.19660150224.
[34] R. Chandiramouli, B.G. Jeyaprakash, "Review of CdO Thin Films" Solid State Sciences. 2013, 16, 102-110. https://doi.org/10.1016/j.solidstatesciences.2012.10.017.
[35] Zainab N. Jaf, Zhong-Tao Jiang, Hussein A. Miran, Mohammednoor Altarawneh, Jean-Pierre Veder, Manickam Minakshi, Zhi-feng Zhou, H.N. Lim, N.M. Huang, Bogdan Z. Dlugogorski "Physico-Chemical Properties of CrMoN Coatings - Combined Experimental and Computational Studies" Thin Solid Films. 2020, 693, 137671. https://doi.org/10.1016/j.tsf.2019.137671.
[36] Zainab N. Jaf, Zhong-Tao Jiang, Hussein A. Miran, Mohammednoor Altarawneh "Thermo-Elastic and Optical Properties of Molybdenum Nitride", Can. J. Phys. 2016, 94, 902. https://doi.org/10.1139/cjp-2016-0125.
[37] R. H. Ritchie "Plasma Losses by Fast Electrons in Thin Films", Phys. Rev. 1957, 106, 874. https://doi.org/10.1103/PhysRev.106.874.

[DOI: 10.22068/ijmse.3991]